

PHYSICAL REVIEW D

PARTICLES AND FIELDS

THIRD SERIES, VOLUME 31, NUMBER 3

1 FEBRUARY 1985

Search for heavy charged particles and light nuclei and antinuclei produced by 400-GeV protons

J. L. Thron,* T. R. Cardello,† P. S. Cooper, L. J. Teig, and Y. W. Wah‡
J. W. Gibbs Laboratory, Yale University, New Haven, Connecticut 06511

C. Ankenbrandt, J. P. Berge, A. E. Brenner, J. Butler, K. Doroba,§ J. E. Elias, J. Lach,
P. Laurikainen,** J. MacLachlan, and J. P. Marriner
Fermi National Accelerator Laboratory, Batavia, Illinois 60510

E. W. Anderson and A. Breakstone
Department of Physics, Iowa State University, Ames, Iowa 50011

E. McCliment
Department of Physics, University of Iowa, Iowa City, Iowa 52242
(Received 11 June 1984; revised manuscript received 1 November 1984)

The results of a search for the production of heavy charged particles in 400-GeV proton collisions in copper are presented. The experiment was sensitive to particles of mass 4 to 12 GeV/ c^2 having lifetimes $\geq 3 \times 10^{-9}$ sec. No particles of this type were observed. A 90% confidence limit of 2.5×10^{-36} cm²GeV⁻²nucleon⁻¹ is placed on the invariant production cross section for negative particles, and a similar limit of 10^{-35} cm²GeV⁻¹nucleon⁻¹ for positively charged particles. In addition, the production of the deuteron, antideuteron, and triton were measured using the same apparatus.

I. INTRODUCTION

We report on a search performed at Fermilab, E-497, to look for the existence of new, massive (≥ 4 GeV/ c^2) charged particles. The experiment was performed in a negative 86-GeV/ c secondary beam produced by 400-GeV protons incident on a copper target. The relatively short length of the experiment, less than 20 m from the production target to the final detector, using Cerenkov counters with a momentum-analyzed beam, allowed direct electronic observation of new particles with short lifetimes. Previous direct-measurement searches¹⁻⁴ using time-of-flight measurements to determine the particle's velocities required long flight paths (230 to 1100 m) to achieve separation of different particles. A similar search⁵ for massive, neutral particles used a flight path of 590 m with a calorimeter to determine timings and particle energies. Although most of the data were taken using a negative secondary beam of 86-GeV/ c momentum, data were also taken at lower momenta where the production of known nuclei were within the detection range of our apparatus. Some data were also taken with a positive secondary beam. The complete set of runs is shown in Table I.

In this experiment, Cerenkov counters were used to reject low-mass particles. The momenta of the remaining

particles were calculated by observing their deflection by a magnetic field. Their velocities were measured by a Cerenkov counter. These values along with their measured momenta enabled their masses to be calculated.

Theoretical and experimental motivations exist for searching in this lifetime-mass region. Among the suggested particles are massive integrally charged quarks,^{6,7} color-sextet fermions,⁸ six-quark states,⁹ and pion-neutron

TABLE I. Types of data runs, showing the total pion flux through the experiment for that type of run. Also shown is the secondary momentum chosen for the study. In all cases the primary beam was at 400 GeV.

Particle type	Pion flux	Momentum (GeV/ c)
Negative heavy mass	3.0×10^{10}	86.8
Positive heavy mass	0.6×10^{10}	86.8
Antideuterons	2.9×10^9	31.2
Deuterons	7.0×10^8	31.2
Tritons	2.5×10^9	47.6
³ He	1.6×10^9	27.8

bound states.¹⁰ Calculations for the lightest supersymmetric particles containing gluinos indicate^{11,12} that their lifetime and mass might be in the sensitive range of this experiment. In addition, there have been persistent reports^{13,14} of massive charged particles observed in cosmic-ray time-of-flight experiments.

To calibrate the particle-search experiment and also since it is of interest in its own right, the production of known particles was also measured. Most of these data were the observation of antideuterons. Their production rate relative to pions was measured and, after correcting for their relative absorptions,¹⁵ a production cross section was determined. This can be compared to a number of other measurements^{16,17} at various Feynman x and transverse momenta. Similar, but less accurate production measurements were made for deuterons and tritons.

II. EXPERIMENTAL APPARATUS

A. Beam, target, channel

This experiment was performed in the Fermilab Proton Center beam line using an incident beam of 400-GeV protons. The proton beam was focused to a size of less than $1 \times 1 \text{ mm}^2$ at the target. The incident protons were delivered to the experiment during a 1-sec beam pulse with a repetition rate of approximately 10 sec. The primary beam rate limit of 4.0×10^{10} particles/pulse in this experiment was set by the instantaneous secondary beam rate in the proportional wire chambers (PWC's).

The copper target was 2 mm by 2 mm in cross section. For most runs, it was one absorption length (14.8 cm) long and was mounted so that it could be moved completely out of the beam remotely. The target was centered in the entrance aperture of a 7-m-long curved magnetic channel. The channel deflected the secondary beam by 21 mrad and is depicted in Fig. 1. The first section of the channel (198 cm) contained the target and a beam-dump region. The dump absorbed particles emitted by the tar-

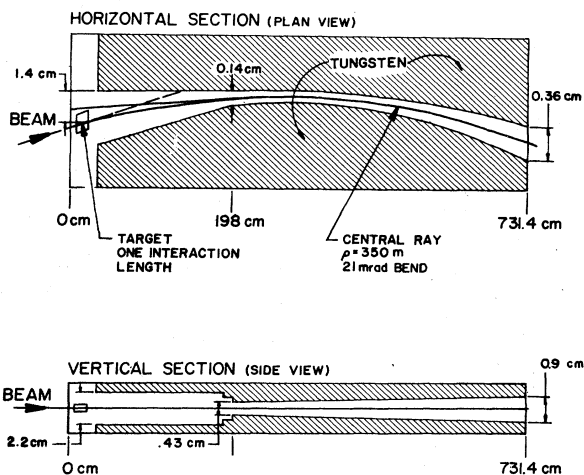


FIG. 1. Momentum-selecting channel. (Not to scale.) The noninteracting beam is dumped in the enlarged upstream section of the channel.

get which were not in the channel phase space as well as any uninteracted beam particles. The channel walls defined the beam phase space and were made of sintered tungsten (90% W, 6% Ni, 4% Cu) having a density of 17.08 g/cm^3 . In this geometry, the angle of the incident proton beam was adjusted so that the central ray corresponded to 0-mrad particle production.

The channel was in a $7.0 \times 3.0 \times 1.7\text{-m}^3$ (length \times width \times height) dipole magnet. At maximum current the magnet produced a field of 35 kG in the region of the channel. By varying the current and polarity of the magnet, one could select singly charged particles of either sign with momenta up to 350 GeV/c exiting the channel. This system produced a secondary beam with a full-width momentum spread of $\Delta p/p = \pm 7\%$ and a solid angle of $0.64 \mu\text{sr}$. A more detailed discussion of the channel design and construction is given by Cardello.¹⁸

About 500 000 particles per pulse were normally maintained within the secondary beam phase space. Total rates two to three times higher than this were observed when all the particles passing through the apparatus were included. This excess was mainly due to muons coming through the magnet iron and low-momentum particles being produced by interactions of the beam in the walls of the downstream sections of the channel.

B. Proportional wire chambers and scintillation counters

The trajectories of particles exiting the channel were determined by two clusters of PWC's before the spectrometer magnet and two following it. These are shown in Fig. 2 as PWC's *A*–*D*. Clusters *A*, *B*, and *D* had wire planes¹⁹ which gave a position measurement in the *X* (horizontal), *Y* (vertical), and *U* (45°) directions; the *C* chamber had only *X* and *Y* planes. The wire planes in the *A*, *B*, and *C* clusters had an effective wire spacing of $203 \mu\text{m}$. This was accomplished by using a pair of planes each with $406\text{-}\mu\text{m}$ spacing staggered with respect to each other. Cluster *D* had only single planes of $406 \mu\text{m}$ spacing in *X* and *Y*. Nineteen wire planes were contained in the total system. The effective area of the chambers was contained in a 2.5-cm-diameter circle. The measured resolution of these chambers is consistent with the expected value of the effective wire spacing divided by $\sqrt{12}$. These chambers²⁰ were capable of handling particle rates up to $\approx 1 \text{ MHz}$.

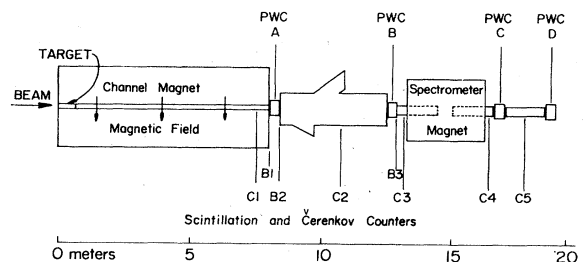


FIG. 2. A side view of the experimental equipment. Shown are the hyperon magnet and channel, the spectrometer magnet, the trigger scintillation counters (*Bi*), the Čerenkov counters (*Ci*) and the PWC clusters.

Three plastic scintillation counters $B1$, $B2$, and $B3$, matched to the size of the PWC's, further defined beam particles spatially as well as temporally. Additional scintillation counters (not shown in Fig. 2) were used in anticoincidence to reject particles outside the expected beam phase space. These included four counters on the upstream face of the $C2$ Čerenkov counter to reject particles which would pass through the more sensitive part of its phototubes. Two other counters with holes sufficiently large for the beam to pass through them (called halo counters) insured that beam particles passed through the active area of the PWC's. Finally, four other scintillation counters which could be remotely positioned into the beam proved useful as diagnostic tools.

C. Čerenkov counters

Four Čerenkov counters were used to tag particles as heavy or light; a fifth actually measured their velocity. These counters fell into three categories: threshold counters ($C1, C4$) giving a signal for low-mass particles, dual-channel counters ($C3, C5$) which could produce a separate signal for either low- or high-mass particles, and a broadband counter ($C2$) to measure the particle's velocity. Combining this with momentum information determined the mass of the particle. The Čerenkov-counter positions are shown in Fig. 2.

1. Threshold Čerenkov counter $C1$

The $C1$ Čerenkov counter (Fig. 2) used the last 75 cm of the channel as its radiating volume. This volume was sealed with 1 mil aluminum windows, and Freon (dichloro-tetrafluoro ethane, $C_2Cl_2F_4$) gas at atmospheric pressure flowed through it. At the downstream end, outside of the channel, an aluminized plastic film reflected the Čerenkov radiation via an aluminized light pipe onto a high-sensitivity (RCA 31000M) photomultiplier. The light pipe was long enough to ensure that the phototube was in region of low magnetic field. Two outputs were taken from the base of the phototube. One was used for the fast trigger logic and the other was analyzed by an analog-to-digital converter (ADC). The threshold for Čerenkov radiation for this counter was a particle with a relativistic γ of 18.6, corresponding to a pion momentum of 2.6 GeV/c.

2. Threshold Čerenkov counter $C4$

The threshold counter $C4$ was designed to reject pions. The radiating gas was N_2 at 65 psia, which set the threshold mass at 3.75 GeV/c². The counter was mounted on the downstream end of the spectrometer magnet and extended into the magnet aperture.

Figure 3 shows a sectional view of $C4$. The beam entered through a stainless steel window (0.08 g/cm²), traversed the radiating medium (0.75 g/cm²) and exited through a final window. The Čerenkov radiation was reflected from a 45° planar mirror on a spherical mirror at the top of the vertical section. The spherical mirror focused the Čerenkov radiation back through a hole in the center of the 45° mirror onto a quartz lens just before the

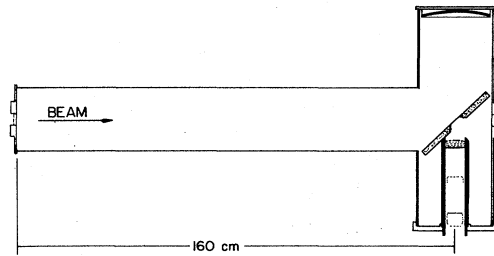


FIG. 3. Threshold Čerenkov counter $C4$ for vetoing fast particles. The primary mirror is the 45° planar mirror on the right. The spherical mirror on the top right focused the Čerenkov light onto the RCA 31000M photomultiplier mounted in the housing in the lower right of the diagram.

(RCA 31000M) photomultiplier. The quartz lens, coated with 54-nm MgF_2 , served both as a pressure seal window and a final focusing element. All mirrors were coated with 100-nm aluminum and 25-nm MgF_2 . At the operating pressure, the mean Čerenkov angle for pions was 50 mrad.

3. Dual-channel counters $C3$ and $C5$

The dual-channel counters $C3$ and $C5$, shown in Fig. 4, were designed to be sensitive to Čerenkov radiation from particles with mass up to 6 GeV/c² at beam momenta of 75 GeV/c. The 100-cm-long radiating medium was nitrogen at 173 psia and was adjusted to place the discrimination cut between high- and low-mass channels at 4 GeV/c². $C3$ was mounted on the upstream face of the spectrometer magnet with part of the counter extending into the magnet field. $C5$ was placed at the end of the experimental beam line. The entrance and exit windows were 25- μ m stainless steel. After passing through a thin area in the 45° planar mirror, the beam entered the radiating volume. Light produced here was focused by a 48-in.

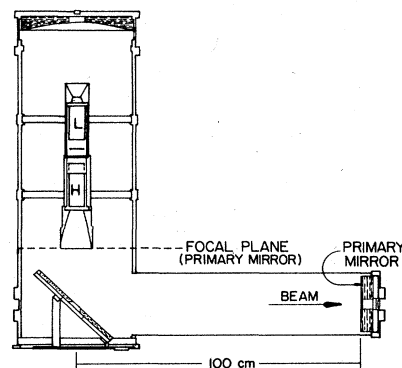


FIG. 4. Dual-channel Čerenkov counters $C3$ and $C5$. The primary (spherical) mirror focused the Čerenkov light for heavy-mass particles, after reflection from the 45° planar mirror, into the lower light-collecting cone. Light from lower-mass particles was collected by the spherical mirror on the upper left of the diagram and focused into the upper light-collecting cone.

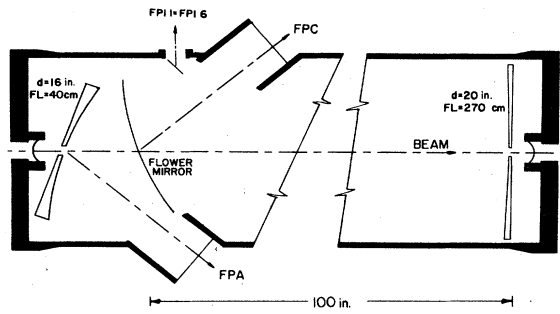


FIG. 5. Čerenkov counter C2 for measuring the velocities of the particles. The primary (parabolic) mirror, on the right, focused the Čerenkov light onto the flower mirror. The light intercepted by that mirror was collected in the FPC channel. That which was not intercepted by the flower mirror was collected by the FPA photomultiplier after reflection from the spherical mirror on the left. Light from low-mass particles was sampled by small 2-in. \times 2-in. mirrors mounted at 45° and reflected onto the six photomultipliers FP1 through FP6.

focal-length spherical (primary) mirror coated with 100-nm aluminum and 25-nm MgF₂.

The Čerenkov radiation, after reflection by the 45° mirror, was brought to a ring focus at the bottom edge of the iron phototube enclosure. Light from heavier mass particles entered a light collecting cone and was directed to phototube H. Light from lighter particles passed outside of this light collecting cone, were reflected from a spherical mirror at the top of the counter and entered phototube L. The phototubes were isolated from the high-pressure gas volume by 1-in.-thick quartz windows coated with 54-nm MgF₂. To correct for ambient magnetic fields, each phototube (RCA 31000M) was magnetically shielded and wound with a compensating coil.

4. Velocity measuring Čerenkov counter C2

The C2 counter, shown in Fig. 5, was capable of measuring a particle's velocity over a limited range. The pressure vessel body was a steel pipe, internally blackened, and filled with nitrogen as the Čerenkov radiating medium. The entrance and exit of the beam from the counter was through 25- μ m stainless-steel windows.

The high-sensitivity photomultipliers (RCA 31000M) observed the Čerenkov light produced in the counter through quartz windows in the pressure vessel. The nitrogen pressure could be varied from 0 to 300 psia to change the observed light ring radius for a given particle velocity.

The Čerenkov light was focused to a ring image by the downstream parabolic mirror. The image was produced near the face of the middle mirror, the "flower mirror." This mirror, illustrated in Fig. 6, was designed to reflect a portion of the light and transmit the rest to the upstream mirror. Light reflecting from the flower mirror was collected in the top phototubes (FPC) while the transmitted light went to the bottom phototubes (FPA) via the back mirror. Both phototubes were fitted with compound parabolic cones for optimum light collection.²¹ A light ring of larger radius would have a larger proportion of its pho-

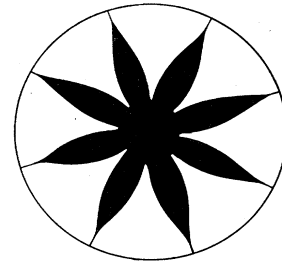


FIG. 6. The flower mirror in C2; the white areas are reflecting, aluminized sections of a parabolic mirror, while the black regions are cut away to allow light to pass through.

tons reflected to the upper phototube FPC while a smaller ring would go predominantly to the lower phototube FPA. Thus by comparing the two analog signals a measure of the radius was obtained.²² Figure 7 shows the angular resolution of the flower-mirror system. It was obtained by reducing the pressure in C2 until the Čerenkov light from pions fell on the flower mirror.

Čerenkov light rings of radius larger than the outer edge of the flower mirror were partially collected by six planar mirrors distributed around the flower mirror, which reflected the light onto the faces of six corresponding phototubes, FPI1–FPI6. These signals were used to veto low mass particles (mostly pions). For clarity, Fig. 5 shows only one of these six mirrors.

D. Spectrometer magnet

The spectrometer magnet was 72 in. long in the beam direction and had a vertical gap of 10 in. and a 24-in. width. It gave a momentum resolution $\Delta p/p$ of approximately 1%. For these measurements, the spectrometer

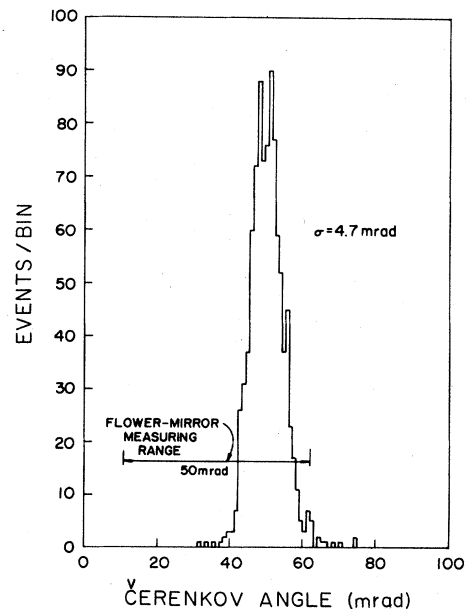


FIG. 7. Angular resolution of the flower-mirror system. Here σ is the standard deviation.

magnetic imparted a transverse deflection of ≈ 0.4 GeV/ c and operated in a range of magnetic fields which were directly proportional to the current.

III. EXPERIMENT CALIBRATION

A. Momentum

In order to determine the particle's momentum, it was necessary to know the magnetic field integral of the spectrometer magnet. This was measured quite accurately by another experiment²³ which used the same magnet and power supply. During that experiment, charged particles with known momenta were tracked through the magnet. The field integral was found to be a linear function of the magnet current in the region used in this experiment. Thus, given the magnetic field value, the momentum of the particles emitted by the channel could be determined.

B. Čerenkov counters

The radiating gas in C1 was chosen so that a low-mass particle would produce approximately 10 photoelectrons at 86 GeV/ c . The Čerenkov angles in the four other counters were adjusted by controlling the pressure of the nitrogen gas. In C4 this was to set the Čerenkov threshold while in C2, C3, and C5 it was to match their geometry with the expected particle responses.

Figures 8 and 9 show the number of photoelectrons N_{PE} as a function of the gas pressure for several of the counters. For C4 (Fig. 8) the functional dependence of the response is

$$N_{PE} = 2N_0L\delta P.$$

Here P is the gas pressure, δ is the index of refraction (n) minus one per unit pressure ($\delta P = n - 1$), L is the length of the Čerenkov-radiating medium, and N_0 is a measure

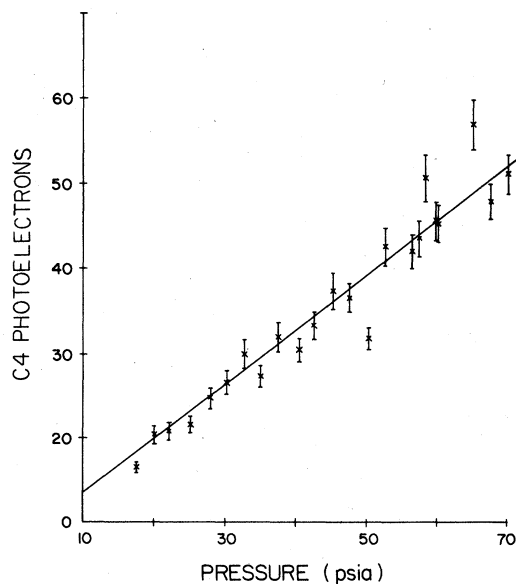


FIG. 8. C4 response curve.

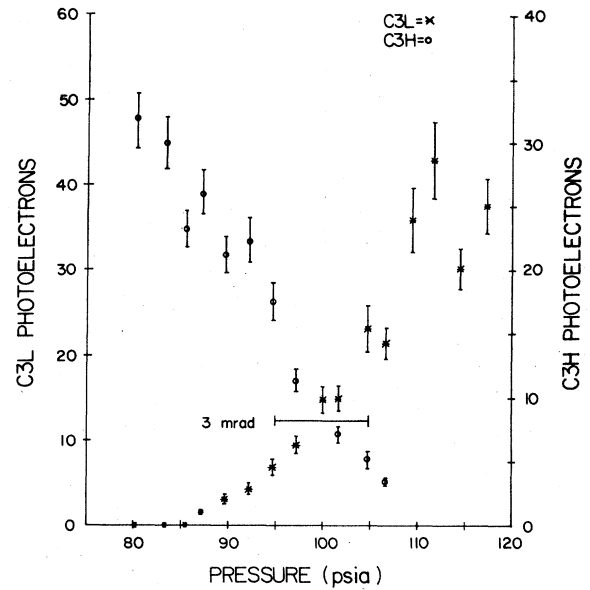


FIG. 9. C3 response curve in the region of the high- and low-mass channel crossover. The expected overlap range of 3 mrad is indicated.

of the counter's efficiency. N_0 is determined to be ≈ 96 cm^{-1} .

The response of one of the dual-channel counters is shown in Fig. 9. Plotted here is N_{PE} for each of the two channels (H and L) as a function of gas pressure. Note that the position where the two distributions cross gives a useful check of the geometry.

For the counter C2, the response had to be quantified so that the mass of a particle could be determined from its signal. From the mirror shape it was expected that the radius r of the Čerenkov-light ring is given by

$$r = \frac{1}{2}(r_1 + r_2) + \frac{1}{\pi}(r_1 - r_2)\sin^{-1}\alpha,$$

where

$$\alpha = (g_0C - A)/(g_0C + A).$$

A and C were the magnitudes of the signals from the phototubes FPA and FPC viewing the flower pattern, g_0 was the relative gain of the two light-detection systems, and r_1 and r_2 (1.9 and 17.8 cm, respectively) were the inner and outer radii of the flower pattern shown in Fig. 6. A detailed study of the angular-resolution curves, such as the one shown in Fig. 8, as a function of gas pressure (hence, the Čerenkov angle) indicated an anomalous behavior. This behavior could be explained if it was assumed that the flower mirror was not concentric with the Čerenkov-light ring. An offset of 4.9 cm was sufficient to make all of the data consistent. This offset meant that rings of light which would have fallen off the inside or outside of the flower mirror still gave meaningful signals. The ring offset was caused by a misalignment of the imaging mirror and by the beam's passing through the counter slightly off the axis of the mirror. Coulomb scattering of the

charged particles, the aberrations caused by the mirror's tilt and the chromatic dispersion of the Čerenkov light increased the width of the Čerenkov ring. All these factors contributed to a somewhat degraded resolution and gave rise to a wider angular acceptance of the system. To check these effects, the flower-mirror system was used to calculate the mass of the antideuteron events. The result, Fig. 10, shows agreement with the known mass within the errors.

IV. DATA ACQUISITION

For most runs, two basic trigger types were used. The first, designated BUPS (beam upstream), was simply an indication that a particle had come down the middle of the upstream portion of the apparatus. The second was a BUPS trigger with the added restriction that the trigger particle not have a low mass, called GBLB (good beam, low mass bar). Typically, the BUPS trigger had three basic components. These included a coincidence of three beam defining scintillators and a veto from selected halo scintillators. The third requirement incorporated special logic (called the beam rationer) which allowed events with a second beam particle in temporal proximity to the first to be rejected. This time could be adjusted so that only one beam particle came within the resolving time of the PWC's.

The GBLB trigger was a BUPS signal with the possibility of a veto from the low-mass-detecting Čerenkov counters. In most runs, only the vetos from the upstream counters, C1 and FPI1–FPI6, were used in the on-line trigger.

The two trigger types each went through separate pre-scalers which were adjusted to produce approximately equal numbers of the two triggers. The prescaled signals

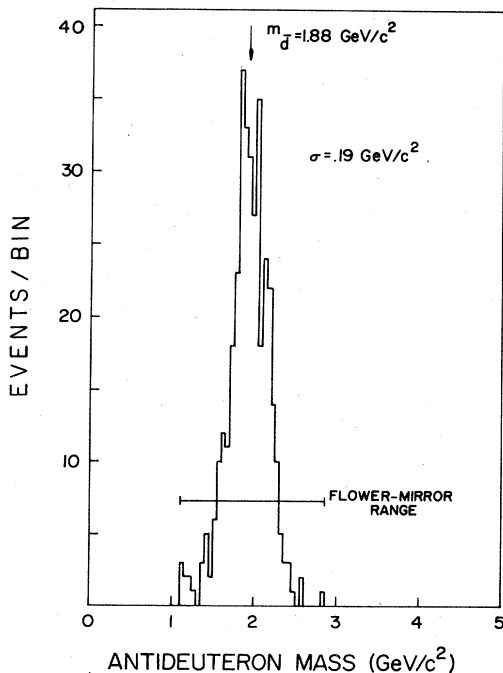


FIG. 10. Antideuteron mass as computed from C2.

were then used to trigger the ADC's, the latches, and the PWC's and to start the computer's data acquisition.

The ADC's recorded pulse-height information from all of the Čerenkov counters and some of the scintillators. The latches stored the state of all the trigger defining scintillators, all the veto scintillators and the Čerenkov counters. These as well as PWC information were recorded for each trigger.

The experiment used a Digital Equipment Corporation PDP 11/45 computer, running the Fermilab MULTI program,²⁴ which acquired the data for each event from a CAMAC-based data-acquisition system. All triggered events were written onto magnetic tape. The computer system performed on-line diagnostics and analysis as well as some event reconstruction.

The data runs were set up to detect a variety of particles, of assumed charges and masses. This was done by choosing a momentum for the secondary particles to maximize the production cross section, usually at Feynman $x=0$ for that particle. Then the Čerenkov-counter pressures were set to separate this particle from lower-mass ones, in the case of C3, C4, and C5, and to center the expected mass within the acceptance of the measuring range for C2. (See Table I). The rates at which data were actually recorded on tape varied from about 20 per pulse for the particle-search runs, to several hundred per pulse for pion runs.

V. DATA REDUCTION

A. Tracking

The tracking procedure was designed to pick out events which passed through the apparatus in a manner consistent with a single particle which did not decay or significantly deviate from a noninteracting trajectory. All events which were on tape had necessarily passed the BUPS trigger requirement. This already gave a fairly clean beam in the upstream portion of the experiment. The exact path of the particle, as well as its momentum, was determined by the PWC's. Two cuts could be made once the hit positions had been determined. Using the *A* and *B* clusters the track could be extrapolated backward to the production target and forward to the *D* cluster. This extrapolation used the mean momentum for the particles and so was not exact. The first cut required that the forward extrapolated track match the data in the *D* cluster within 6.5 mm vertically and 9 mm horizontally. If no valid *D* cluster hits were recorded, no cut was made. The backward extrapolation required the track to intersect the target within 8 mm in the vertical direction. The *D* cluster cut eliminated events which had momenta substantially different from the mean. Usually these were low-momentum particles produced at the end of the channel or in the apparatus, or particles which decayed into lower momentum secondaries.

A least-squares fit, weighted with the PWC measurement errors, was made on the hit coordinates. A 10^{-5} confidence level cut was placed on this fit.

For the antideuteron runs, after the track fitting, a double peak was observed in the momentum spectrum (see

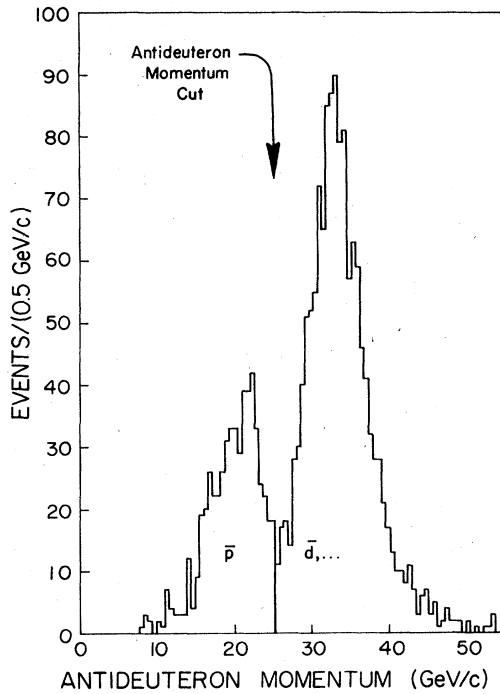


FIG. 11. Momentum distribution of an antideuteron run, showing the cut used to reject the antiprotons.

Fig. 11). The lower peak was approximately half the momentum of the higher peak and was well below the lowest momentum in the channel emittance. These events were interpreted as the low-momentum tail of the antiprotons coming from the channel. They were produced by interactions in the last part of the channel creating an antiproton which left the channel and entered the experiment instead of being absorbed in the channel's tungsten walls. Another possible source of these antiprotons was from the dissociation of antideuterons. The antiprotons with approximately one half the channel momentum were then selected by the trigger since their velocities were identical to the higher momentum, heavier antideuterons when measured by the trigger Čerenkov counters.

The possibility that this secondary peak was a computational or an instrumental effect was eliminated by looking at the heavy-mass search (see Fig. 12) and the pion runs where no such peak was seen. To obtain a pure antideuteron sample, a cut was placed on the momentum distribution to keep only those events with a momentum greater than 25.5 GeV/c. The particle-identification efficiency of these runs relative to others was not biased since such a cut had practically no effect. The deuteron and triton runs exhibited a similar problem. However, the tritons were harder to separate from their backgrounds since these included not only protons but also deuterons near the triton momentum.

B. Cuts on Čerenkov-counter data

The Čerenkov-counter signals were used to distinguish low-mass from high-mass particles. The antideuteron

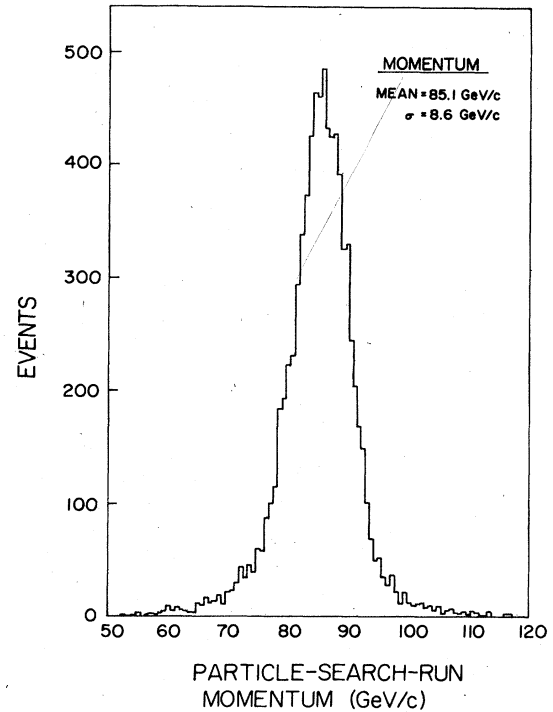


FIG. 12. Momentum distribution for a heavy-particle-search run.

runs were used to determine values for the cuts, since the antideuterons were produced in sufficient quantities to provide a clear signal. Counter C1, which had been used in the trigger, was not used again in the off-line analysis. The C4 pulse-height distribution showed a clean separa-

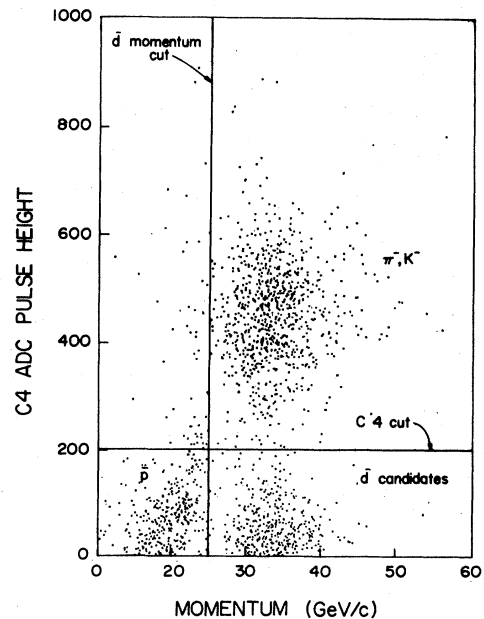


FIG. 13. C4 pulse height versus momentum for an antideuteron run, showing the C4 pulse-height cut to reject fast particles and the momentum cut to reject antiprotons.

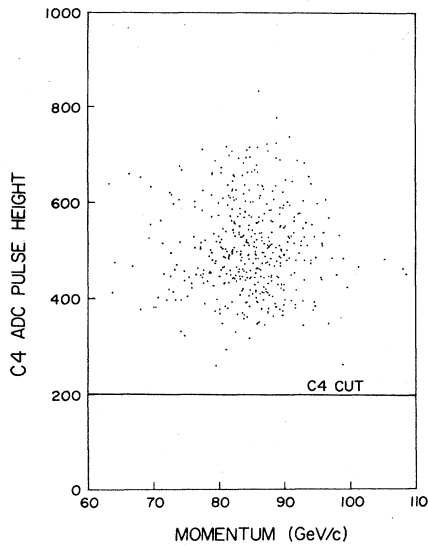


FIG. 14. C4 pulse height versus momentum for a heavy-particle-search run, showing the C4 pulse-height cut to reject low-mass particles.

tion between the two peaks where the cut was placed. Figure 13 shows the C4L pulse height versus momentum for an antideuteron run. The one-half-momentum antiprotons are clearly visible, trailing into the "light"-particle area as their momentum rises. The previously mentioned momentum cut is also shown. Figure 14 shows a similar plot for a heavy mass search run.

For C3, a scatter plot of C3L versus C3H accentuated the separation, with the cut placed diagonally as indicated. Figure 15 is from an antideuteron run and Fig. 16 is from a heavy mass search run. The C5 data was treated

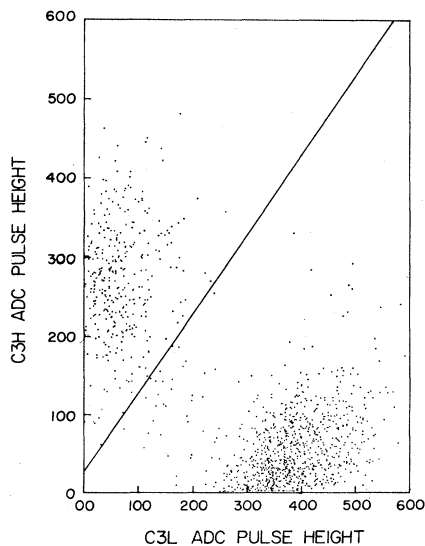


FIG. 15. C3H versus C3L for an antideuteron run showing the clean separation of the antideuterons from the faster particles and the cut applied to reject the latter.

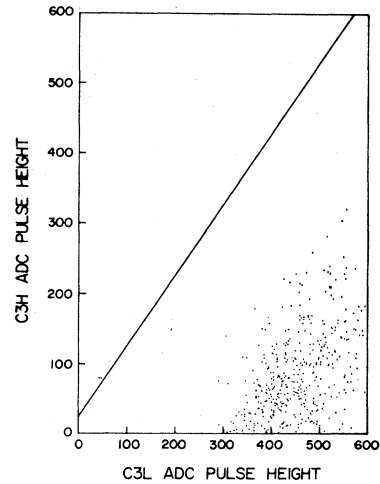


FIG. 16. C3H versus C3L for a heavy-particle-search run showing the cut to reject the low-mass particles.

identically. This was justified since the design and operating conditions were the same and experimentally the two counters exhibited similar pulse-height distributions. The FP1-FP6 counters in C2 were used only in the on-line analysis. FPC and FPA were not used to reject low-mass particles since this might have biased their mass measuring ability. The efficiency of the various counters for identifying antideuterons could then be determined for the given cuts by comparing one to the other two (see Table II). After these cuts, most of the heavy mass candidates lay close to an exact diagonal on the C3 and C5 scatter plots, in particular $C3L = C3H$ and $C5L = C5H$. This was surprising since antideuteron plots had shown almost no population there.

Sudden changes in the electrical ground level between the experiment and the counting room had been observed. These could explain the spurious signals to the ACD's as well as to the scintillator discriminators which would have had to have produced a trigger. In fact, looking at the scatter plots for C3 and C5 before the tracking cuts, there was a definite enhancement along the diagonal (see Fig. 17). It was observed that these events occurred in both the C3 and C5 counters at the same time. Figure 18 shows a scatter plot of $(C5H - C5L)$ versus $(C3H - C3L)$ under the same conditions as Fig. 17. The diagonal clusterings would project to accumulations of events at zero on each axis. The clustering in the center indicates a strong correlation between the two counters for these

TABLE II. The efficiency of the Čerenkov counters for correctly identifying an antideuteron with the cuts as described for the antideuteron runs.

Counter	Efficiency
C3	100.0±0.5%
C4	96.8±1.1%
C5	97.6±1.0%
Total	94.5±1.5%

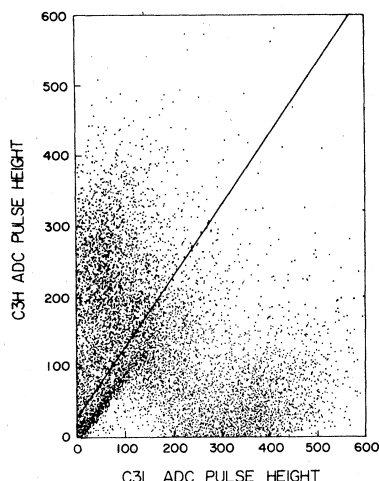


FIG. 17. $C3H$ versus $C3L$ for an antideuteron run with no PWC tracking required, showing the diagonal band of electronic noise and the cut used to reject it.

events. The spread along $C3H - C3L$ comes from low-momentum particles which produce a signal in $C3$ and do not get through the spectrometer magnet, therefore producing only pedestals in the $C5$ ADC's. This indicated that the signals were caused by electrical noise since these counters had in common only the power supplies and some modules in their electronics systems. To remove this background, a tighter cut were placed on $C3$ and $C5$ as shown in Fig. 17. This cut was not used for the antideuteron runs. Here the expected number of events where the electrical noise coincided with a real particle track was negligible compared to the antideuterons rate. The efficiency of the counters was therefore somewhat reduced in detecting the high-mass particles (see Table III).

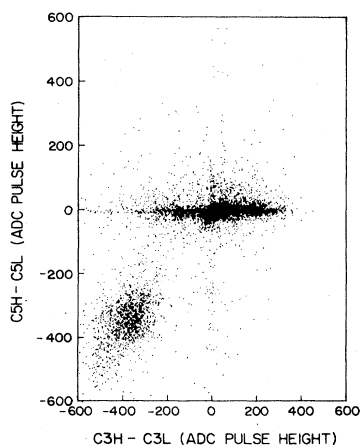


FIG. 18. $C5H - C5L$ versus $C3H - C3L$ for an antideuteron run, showing the strong correlation between the two independent counters of the electronic noise.

TABLE III. The efficiency of the Čerenkov counters for correctly identifying a high-mass particle with the cuts as described for those runs.

Counter	Efficiency
C3	$98.6 \pm 0.9\%$
C4	$97.6 \pm 1.1\%$
C5	$87.7 \pm 2.3\%$
Total	$84.4 \pm 2.5\%$

VI. RESULTS

A. Antideuterons

A total of $(4.60 \pm 0.07) \times 10^3$ antideuterons passed the analysis cuts. A number of corrections had to be applied to obtain a \bar{d}/π^- production ratio. These corrections are enumerated in Table IV. To get the number of pions observed, N_π , the reconstructed BUPS triggers were examined. They were composed of particles which passed straight through the experimental apparatus satisfying the upstream scintillator trigger and which passed the off-line tracking cuts. The approximate composition of this beam was²⁵ 88% pions, 10% kaons, and $\approx 2\%$ antiprotons. With the assumption that the PWC tracking was the same for any minimum-ionizing charged particle, one gets $\pi^-/\text{BUPS} = 0.88$. Thus, for a given run,

$$N_\pi = N_{\text{BUPS}} 0.88 \times 2^{(\text{BUPS prescale factor})},$$

where N_{BUPS} is the number of BUPS triggers, gives the number of reconstructed pions passing through the apparatus during that run. A total of $(1.66 \pm 0.02) \times 10^9$ pions were observed in association with the observed antideuterons.

It was assumed that the PWC tracking efficiency was the same for pions and antideuterons. The relative acceptance of the two particles in the apparatus was also taken to be unity.

The Čerenkov counters were not used in the BUPS determination, so their efficiency was, in effect, 100%. The number of antideuterons was affected by the Čerenkov counters' efficiencies and by the cuts applied to their signals. The efficiency of the three counters which

TABLE IV. Corrections applied to the observed antideuteron-to-beam ratio to obtain an antideuteron-to-pion production-cross-section ratio.

Description	Correction
Nondecay π^-	0.95 ± 0.01
Nondecayed \bar{d}	
Relative absorption in apparatus (\bar{d}/π)	1.27 ± 0.01
Relative reabsorption in target (\bar{d}/π)	1.54 ± 0.05
Relative Čerenkov efficiencies (\bar{d}/π)	0.945 ± 0.15
Relative PWC tracking efficiency	1.0

TABLE V. List of material traversed by the beam in the apparatus and the number of total absorption lengths ($\sigma\rho L$) for antideuterons and pions due to this material.

Nucleus	Mass number	ρL (10^{22} nuclei/cm 2)	$\sigma_{\bar{d}}\rho L$	$\sigma_{\pi}\rho L$
H	1	9.14	0.0107 \pm 0.0006	0.0024 \pm 0.0001
C	12	9.03	0.0483 \pm 0.0025	0.0155 \pm 0.0007
N	14	41.42	0.238 \pm 0.012	0.0800 \pm 0.0037
O	16	1.96	0.0121 \pm 0.0006	0.0042 \pm 0.0002
F	19	0.74	0.0051 \pm 0.0003	0.0018 \pm 0.0001
Al	27	0.84	0.0071 \pm 0.0004	0.0027 \pm 0.0002
Si	28	0.57	0.0051 \pm 0.0003	0.0019 \pm 0.0001
Cl	35	0.37	0.0036 \pm 0.0002	0.0014 \pm 0.0001
Ar	40	0.24	0.0027 \pm 0.0002	0.0010 \pm 0.0001
Fe	56	1.90	0.0256 \pm 0.0013	0.0105 \pm 0.0006
Total			0.358 \pm 0.013	0.121 \pm 0.004

were used to make a positive identification of the antideuterons, C3, C4, and C5, were determined by requiring an antideuteron signal from two of them and counting the fraction of these events which qualified in the third. This was done on an antideuteron run with the actual cuts used. To obtain an overall Cerenkov efficiency it was assumed that the counters' signals were independent of each other. This assumption was not completely true since there was some correlation, but the increased error was small since the individual efficiencies were high. A relative Cerenkov efficiency of 0.945 ± 0.015 was used.

To correct for the pion lifetime, one used the fact that in order for a particle to successfully pass the PWC tracking requirement it had to live to reach a distance, z , of 20 m from the target. Assuming a π^- lifetime of 2.60×10^{-8} sec and a γ of 230, 98.89% survived this distance.

The unequal absorptions of the pions and the antideuterons were accounted for by calculating the amount of each different chemical element in the beam path and obtaining the absorption cross section for pions²⁶ and antideuterons¹³ for these nuclei (see Table V). Summing all these cross sections gave an absorption cross section for the particles passing through the whole apparatus. The results of the fraction surviving were, for the pions 0.8856 ± 0.0035 and for the antideuterons 0.6990 ± 0.0089 .

Finally, a correction was made for particle reabsorption in the target. The number of a given particle observed, N_{obs} , for an incident beam flux on the target, B_{inc} , is given by the equation

$$\frac{N_{\bar{d}}^{\text{obs}}}{B_{\text{inc}}} = n\sigma_{\bar{d}} \int_0^L e^{-\lambda_p z} e^{-\lambda_{\bar{d}}(L-z)} dz.$$

n is the number of nuclei per area in the target, σ is the absorption cross section per nucleus for a given particle, L is the target length, and $1/\lambda$ is the absorption length for a given particle. The \bar{d}/π production ratio is given by

$$\frac{\sigma_{\bar{d}}}{\sigma_{\pi}} = \frac{N_{\bar{d}}^{\text{obs}}(\lambda_p - \lambda_{\bar{d}})(e^{-\lambda_{\bar{d}}L} - e^{-\lambda_p L})}{N_{\pi}^{\text{obs}}(\lambda_p - \lambda_{\pi})(e^{-\lambda_{\bar{d}}L} - e^{-\lambda_p L})}.$$

Using

$$\lambda = 1/\text{absorption length} = \frac{\rho N_A \sigma}{A},$$

where ρ is the density of the material, N_A is Avogadro's number, A is the atomic number, and σ is the absorption cross sections on copper of 1371, 708, and 1270 mb for antideuterons, pions, and protons, respectively. The value of λ is 0.117 ± 0.006 , 0.052 ± 0.003 , and 0.068 ± 0.001 cm $^{-1}$ for the three particle types. This gives a relative correction of 1.5865 ± 0.052 for the run with $L=14.8$ cm. Combining all these correction factors

$$\sigma_{\bar{d}}/\sigma_{\pi} = (5.78\pm 0.13)\times 10^{-6}$$

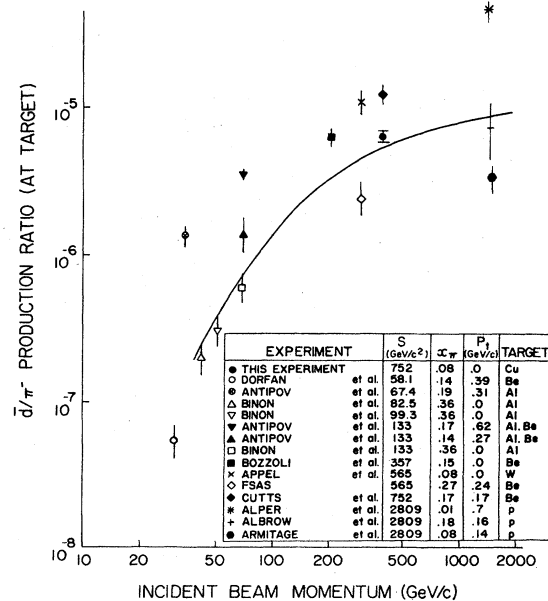


FIG. 19. Compilation of some antideuteron production-cross-section experiments. The line shows the production for antiprotons at half the antideuteron momentum, squared, as a model for the antideuteron. A similar plot originally came from the last entry in Ref. 28.

is obtained for protons on copper at the target. A comparison with previously measured values is shown in Fig. 19. It should be noted that a variety of p_t , x_F , and production target material was used in these experiments and are useful mainly for qualitative comparisons.

B. Heavy particles

Cuts were applied to the negatively charged high-mass search runs which were similar to those used on the negatively charged antideuteron data. After all the cuts had been applied to the high-mass search runs, there were no events left which qualified as heavy particles. This fact was used to calculate a limit on the lifetimes and the production cross sections of such particles. Similar to the antideuteron calculations, the number of pions produced during these runs was counted, appropriate corrections made, and a limit obtained.

The corrections are shown in Table VI. Here, as with the antideuterons, the number of pions was obtained from the number of BUPS triggers. The π^- fraction of the beam²⁵ at this momentum was ≈ 0.9 . The measured invariant pion production cross section²⁷ is 3.19 ± 0.16 mb/GeV²/nucleon. The assumption was made that these heavy particles had the same absorption cross section as the pions. Again the Čerenkov-counter and PWC efficiencies were calculated similarly to the antideuterons. The lifetime correction for the pions and the heavy particles came from an exponential decay which left 99.6% of the pions and $\exp[-ml/(p\tau)]$ of the heavy particles at the end of the experiment. Here m is the mass, τ the lifetime, p the heavy-particle momentum, and l is the length of the experiment. Combining all these factors one gets

$$E \frac{d^3\sigma(m, \tau)}{dp^3} = 6.9 \times 10^{-37} e^{(m/\tau)7.84 \times 10^{-10}} \text{ cm}^2 \text{ GeV}^{-2} \text{ nucleon}^{-1}$$

for a 90% confidence limit on the invariant production cross section for heavy negatively charged particles at $p_t = 0$. These limits are shown in Fig. 20.

Particles in the mass range 4 to 6 GeV/ c^2 could have

TABLE VI. Corrections applied to the heavy-mass-search observations to obtain a production-cross-section limit (1σ).

Description	Correction
Number of massive particles	1 ± 1
Number of π^-	$(1.21 \pm 0.02) \times 10^{10}$
Nondecayed π^-	0.996 ± 0.001
Nondecayed massive particle	$\exp[-(m/\tau)7.84 \times 10^{-10}]$
Relative absorption in apparatus	1
Relative reabsorption in target	1
Relative Čerenkov efficiencies (massive/ π)	0.844 ± 0.025
Relative PWC tracking efficiency	1

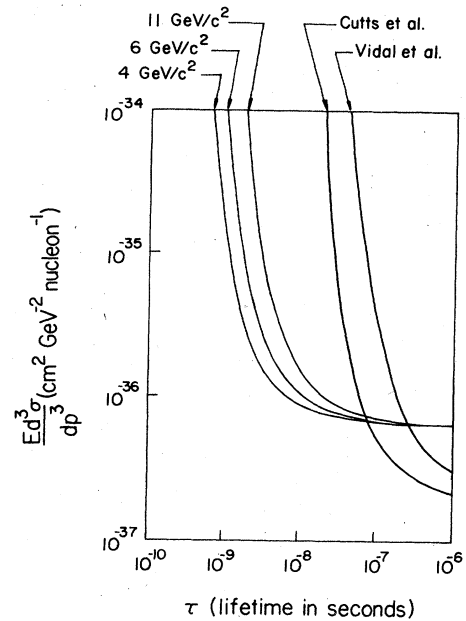


FIG. 20. Limit (90% C.L.) set for negative-heavy-particle production. Regions to the upper right of the curves are excluded. Cutts *et al.* and Vidal *et al.* are data from Refs. 3 and 4, respectively.

been detected and mass measured by the counter C2. However, charged particles with masses up to the kinematic limit, ≈ 11 GeV/ c^2 (≈ 12 GeV/ c^2 if they were not produced in pairs), could also be detected. The signature of one of these particles would be a normal signal in the beam-defining scintillators and the PWC's. Since the particles's velocities would be below the Čerenkov-radiating threshold no signal would be seen in any of the Čerenkov-counter channels. This event would still pass the GBLB trigger requirements since there would be no Čerenkov signal to indicate a light particle to be vetoed. A limit on the production cross section and lifetime of these particles can be calculated (see Fig. 20) in the same way as was done for the 4 to 6 GeV/ c^2 range. In this case, however, the heavy particles are no longer produced near $x_F = 0$ and so their production cross section is expected to be smaller. Although no events of this type were observed, there were a few events which had small values not only for the Čerenkov ADC's, but also for the scintillator ADC's. The mechanism causing such signals is unclear. If these signals were caused by particles traversing the apparatus, they could not be integrally charged. On the other hand, these can be attributed to rare malfunctions of the ADC's.

Most of the high-mass search runs were performed in a negative secondary beam, but some runs were in a positively charged beam. This was achieved by simply switching the polarity on all of the magnets while leaving everything else the same. The positively charged data were analyzed in exactly the same way as were the negative runs. After all the cuts, one possible event remained in the 4 to 6 GeV/ c^2 range. With only one possible event in the sample, the calculation of the cross-section limit for

the production of such heavy particles is independent of the validity of the single event. In order to calculate a limit for the production of heavy-mass positive particles, some of the correction factors had to be changed because the positive particle production cross section was measured relative to π^+ rather than the π^- . The fraction²⁵ of π^+ /BUPS was only 0.75 at these energies. By the same procedure and under the same conditions as for the negative particles this gave

$$E \frac{d^3\sigma(m, \tau)}{dp^3} = 2.8 \times 10^{-36} e^{(m/\tau)7.84 \times 10^{-10}} \text{ cm}^2 \text{ GeV}^{-2} \text{ nucleon}^{-1}.$$

The results are shown in Fig. 21.

C. Other particles

Data was taken to measure the triton production cross section which corresponded to a total incident flux of 2.46×10^9 BUPS. The tritons could not be separated cleanly on the basis of mass. The tails of the much more copiously produced deuterons spread into the triton region. On average, the deuterons had to have $\frac{2}{3}$ of the triton's momentum in order to pass the Čerenkov counter trigger cuts. To take advantage of this fact, a scatter plot of momentum versus mass was examined. As shown in Fig. 22, by this method the tritons could be seen, although the separation was still not very clean. The background of the deuterons in the triton region was estimated as a linearly decreasing tail and was subtracted. This left 32 ± 6 tritons in the sample. Using the same method as for the antideuterons, gave a production ratio $t/\pi^+ = (3.56 \pm 0.70) \times 10^{-8}$. This ratio ignores the differ-

ence in their absorption cross sections since no good measurements exist for the triton and the theories give varying values.

Some data were taken to measure the ^3He production cross section. Since ^3He is doubly charged, it needed twice the normal momentum in order to pass through the momentum selecting channel. Similarly, the spectrometer magnet and the PWC's measured it as having one-half its actual momentum. The angle of the Čerenkov radiation produced depends on mass/momentum of the particle. Therefore, when a mass measurement is made with the counter C2, a ^3He nucleus will produce a signal equivalent to a particle of one-half the ^3He mass with the normal channel momentum. This puts the ^3He mass measurement almost exactly one-half way between the proton and the deuteron signals. Both these particles are produced so much more copiously than ^3He that even using the momentum-mass correlation, as with the triton, and requiring a tighter GBLB trigger (C4 veto and B4, B5) the ^3He signal could not be seen above background.

Deuteron measurements were also made. With an analysis analogous to the antideuterons, a d/π^+ production ratio of $(1.10 \pm 0.19) \times 10^{-4}$ was determined. Reference 29 gives more details of this study.

VII. CONCLUSION

For lifetimes $\geq 3 \times 10^{-9}$ sec, this experiment excludes with 90% confidence limit the production of new heavy negatively (positively) charged particles with invariant cross sections $\geq 2.5(10) \times 10^{-36} \text{ cm}^2 \text{ GeV}^{-2} \text{ nucleon}^{-1}$. The fact that these particles could have been seen regardless of their decay modes, and to a large extent indepen-

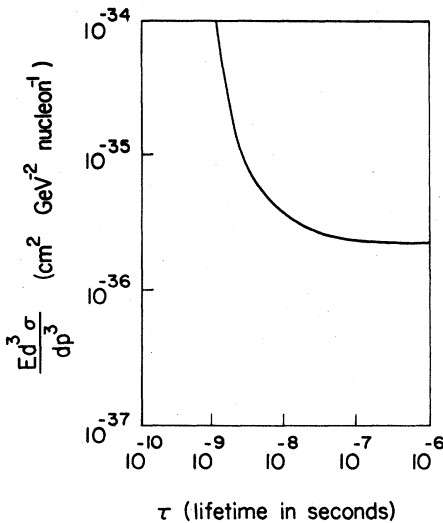


FIG. 21. New limit (90% C.L.) set for heavy-positively-charged-particle production. The curve is for a 6-GeV/c² particle.

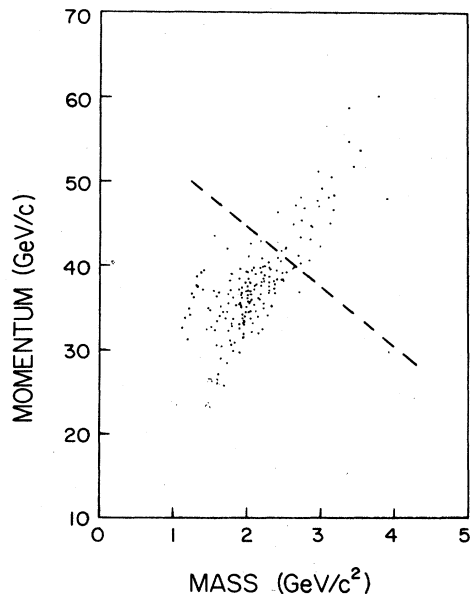


FIG. 22. Momentum versus mass for a triton run showing the triton-deuteron separation.

dent of any of their properties except charge, mass, and lifetime, makes this result an important consideration in future theoretical predictions of new particles.

Although they were not the main purpose of the experiment, and therefore not studied in such detail, the data for the light nuclei and antinuclei may, in combination with other experiments, help produce a better understanding of the mechanisms involved in their production.

ACKNOWLEDGMENTS

We would like to thank Peter Martin, Ed Steigmeyer, Jack Upton, and Mike Catalano for their contributions. We also thank the staff of Fermilab for their help. This work was supported in part by the U.S. Department of Energy under Contract Nos. DE-AC-02-76-CH0-3000, DE-AC-02-76-ER0-3075, and W-7405-ENG-82.

*Present address: HEP Division, Argonne National Laboratory, Argonne, IL 60439.

†Present address: 4159 Islington St., Staten Island, NY 10308.

‡Present address: Enrico Fermi Institute, University of Chicago, Chicago, IL 60637.

§Present address: Institute of Physics, Warsaw University, Warsaw, Poland.

**Present address: Department of High Energy Physics, University of Helsinki, Helsinki, Finland.

¹L. B. Leipuner *et al.*, Phys. Rev. Lett. **31**, 1226 (1973).

²J. A. Appel *et al.*, Phys. Rev. Lett. **32**, 428 (1974).

³D. Cutts *et al.*, Phys. Rev. Lett. **41**, 363 (1978).

⁴R. Vidal *et al.*, Phys. Lett. **77B**, 344 (1978).

⁵H. R. Gustafson *et al.*, Phys. Rev. Lett. **37**, 474 (1976).

⁶M. Y. Han and Y. Nambu, Phys. Rev. B **139**, 1006 (1965).

⁷J. C. Pati and C. H. Woo, Phys. Rev. D **3**, 1173 (1971).

⁸H. Georgi and S. L. Glashow, Nucl. Phys. **B159**, 29 (1979).

⁹S. Fredriksson and M. Jaendel, Phys. Rev. Lett. **48**, 14 (1982).

¹⁰A. Filone, Nuovo Cimento Suppl. **12**, 353 (1954); E. M. Friedlander *et al.*, Phys. Rev. Lett. **45**, 1084 (1980); R. van Dantzig, NIKHEF Report No. PIMU-82-5, 1982 (unpublished).

¹¹I. Hinchliffe and L. Littenberg, in *Proceedings of the 1982 DPF Summer Study on Elementary Particle Physics and Future Facilities, Snowmass, Colorado*, edited by R. Donaldson, R. Gustafson, and F. Paige (Fermilab, Batavia, Illinois, 1982).

¹²M. Chanowitz and S. Sharpe, Phys. Lett. **126B**, 225 (1983).

¹³L. W. Jones *et al.*, Phys. Rev. **164**, 1584 (1967).

¹⁴J. A. Goodman *et al.*, Phys. Rev. D **19**, 2572 (1979).

¹⁵S. P. Denisov *et al.*, Nucl. Phys. **B31**, 253 (1971).

¹⁶D. Cutts *et al.*, in *Proceedings of the Fourth European Sympo-*

sium on $N\bar{N}$ Interactions, Strasbourg, France, 1978, edited by A. Fridman (Éditions du Centre National de la Recherche Scientifique, Paris, 1979).

¹⁷W. Bozzoli *et al.*, Nucl. Phys. **B144**, 317 (1978).

¹⁸T. R. Cardello, Ph.D. thesis, Yale University, 1983; Fermilab Report No. TM-964, 1984 (unpublished).

¹⁹P. A. Souder, J. Sandweiss, and A. A. Disco, Nucl. Instrum. Methods **109**, 237 (1973).

²⁰C. R. Kerns, Fermilab Report No. TM-650, 1976 (unpublished).

²¹H. Hinterberger and R. Winston, Rev. Sci. Instrum. **37**, 1094 (1966); R. Winston, J. Opt. Soc. Am. **60**, 245 (1970).

²²R. Cester *et al.*, IEEE Trans. Nucl. Sci. **NS-25**, 525 (1978); R. Cester *et al.*, *ibid.* **NS-28**, 425 (1981).

²³Y. W. Wah, Ph.D. thesis, Yale University, 1983.

²⁴J. F. Bartlett *et al.*, IEEE Trans. Nucl. Sci. **NS-26**, 4427 (1979).

²⁵K. Doroba, Fermilab Report No. TM-818, 1978 (unpublished).

²⁶A. S. Carroll *et al.*, Phys. Lett. **80B**, 319 (1979).

²⁷F. E. Taylor *et al.*, Phys. Rev. D **14**, 1217 (1976).

²⁸M. G. Albrow *et al.*, Nucl. Phys. **B97**, 189 (1975); B. Alper *et al.*, Phys. Lett. **46B**, 265 (1973); Yu. M. Antipov *et al.*, *ibid.* **34B**, 164 (1971); J. C. M. Armitage *et al.*, Nucl. Phys. **B150**, 87 (1979); T. Binon *et al.*, *ibid.* **30B**, 506 (1969); D. Cutts *et al.*, Phys. Rev. Lett. **41**, 403 (1978); D. E. Dorfan *et al.*, *ibid.* **14**, 995 (1965); Fermilab Single Arm Spectrometer Group, Fermilab Report No. NAL-73/83-EXP (unpublished); References 2 and 17; J. Nassalski and I. Zielinski, Fermilab Letter of Intent, 1979 (unpublished).

²⁹J. L. Thron, Ph.D. thesis, Yale University, 1983.